5-22-2017

Application of Bottlebrush Block Copolymers as Photonic Crystals

Allegra L. Liberman-Martin
Chapman University, libermanmartin@chapman.edu

Crystal K. Chu
California Institute of Technology

Robert H. Grubbs
California Institute of Technology

Recommended Citation

Liberman-Martin, A. L.; Chu, C. K.; Grubbs, R. H. Application of Bottlebrush Block Copolymers as Photonic Crystals. *Macromol. Rapid Commun.* 2017, *38*, 1700058. https://doi.org/10.1002/marc.201700058

Application of Bottlebrush Block Copolymers as Photonic Crystals

DOI: 10.1002/marc.201700058

Feature Article

Application of Bottlebrush Block Copolymers as Photonic Crystals

Allegra L. Liberman-Martin, Crystal K. Chu, Robert H. Grubbs*

_____

Dr. Allegra L. Liberman-Martin, Crystal K. Chu, Prof. Robert H. Grubbs

Arnold and Mabel Beckman Laboratories of Chemical Synthesis, Division of Chemistry and Chemical Engineering, California Institute of Technology, Pasadena, California 91125, United States
E-mail: rhg@caltech.edu

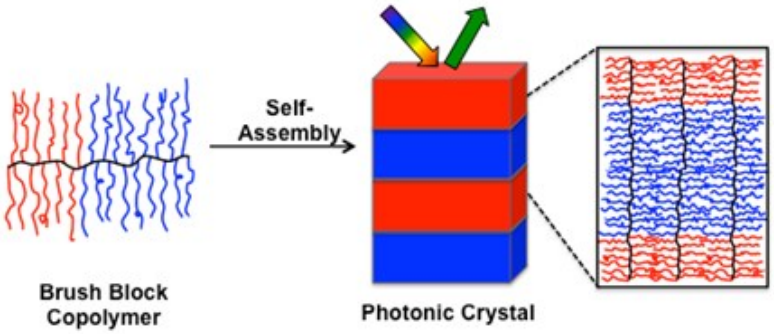

Abstract: Brush block copolymers are a class of comb polymers that feature polymeric side chains densely grafted to a linear backbone. These polymers display interesting properties due to their dense functionality, low entanglement, and ability to rapidly self-assemble to highly ordered nanostructures. The ability to prepare brush polymers with precise structures has been enabled by advancements in controlled polymerization techniques. This Feature Article highlights the development of brush block copolymers as photonic crystals that can reflect visible to near-infrared wavelengths of light. Fabrication of these materials relies on polymer self-assembly processes to achieve nanoscale ordering, which allows for the rapid preparation of photonic crystals from common organic chemical feedstocks. The characteristic physical properties of brush block copolymers are discussed, along with methods for their preparation. Strategies to induce self-assembly at ambient temperatures and the use of blending techniques to tune photonic properties are emphasized.

1. Introduction

Materials that can control and manipulate the flow of light have numerous applications in optical elements, including use as filters,[1] low and high reflection coatings,[2] diffraction gratings,[3] and resonant cavities.[4] One class of nanostructured materials capable of "light processing" is photonic crystals (PCs), which are ordered composite structures with periodicity comparable to the wavelength of light.[5] A requirement for practical applications of photonic crystals is that their bandwidths and center frequencies must be well controlled. Filters and resonant cavities require narrow broadband reflections.[6] In contrast, for coatings that prevent absorption and thermalization of solar energy, broadband reflection (several hundred nanometers) of infrared (IR) radiation is often desired.[7] These diverse demands create the need for methods to produce photonic crystals with varied properties.

This Feature Article focuses on the use of brush polymers, a highly branched polymer architecture, in photonic crystal applications. We highlight specific examples of these materials, with an emphasis on their structures and photonic properties. To introduce this topic, the general properties of photonic crystals and their fabrication will be briefly discussed below. Additional details on coherent light scattering and general fabrication methods for photonic crystals are available in monographs by Joannopoulos et al.[5] and Maldovan and Thomas,[8] as well as in review articles by Yablonovich,[9] Paquet and Kumacheva,[10] Moon and Yang,[11] and Lee et al..[12]

1.1. Properties of Photonic Crystals

The simplest photonic crystal structures consist of alternating layers of high- and low-refractive-index materials.[5] These multilayer assemblies are called one-dimensional photonic

crystals or Bragg stacks. At each interface of these structures, some of the incident light is reflected. Reflections from most wavelengths of light do not add constructively, and thus these wavelengths can propagate through the material. At the specific wavelength for which the optical periodicity of the material matches the path length of a photon, a photonic band gap is formed, which prevents this frequency of light from propagating. At this wavelength, all reflected signals are in phase and add constructively, leading to a reflected signal.

The particular wavelength of light that is reflected (λ) can be described by a combination of Bragg's law and Snell's law (**Equation 1**), where m is the order of Bragg diffraction, d is the layer thickness, η_{eff} is the effective refractive index, and θ is the angle of incidence with respect to the plane of the photonic crystal. The optical path changes with incident angle, causing the band gap to be angle-dependent.

$$\lambda = \frac{2}{m} d \sqrt{\eta_{eff}^2 - sin^2 \theta}$$

(1)

For a normal incident beam (θ = 0), the peak position λ depends on the optical thickness ($n_i d_i$) of each layer in the material as described by **Equation 2**, where n_i is the refractive index of component i, and d_i is the thickness of the ith layer.

$$\lambda = 2(n_1 d_1 + n_2 d_2)$$

(2)

The intensity of the reflected light, or reflectivity (R), for normal incidence for a multilayer film composed of N layers is given by **Equation 3**, for $n_2 < n_1$.

$$R = \left[\frac{1-(\frac{n_2}{n_1})^{2N}}{1+(\frac{n_2}{n_1})^{2N}}\right]^2$$

(3)

These equations form a starting point for control of the reflectance properties of a photonic crystal. Increasing the refractive index contrast or number of bilayers will increase the reflectivity, whereas thickening the layers only affects the wavelength of reflectance.

1.2. Fabrication of Photonic Crystals

A variety of strategies have been developed to prepare photonic crystals. Traditional fabrication has been accomplished by "top-down" techniques such as layer-by-layer stacking,[13] multibeam holography,[14] phase mask lithography,[15] and electrochemical etching.[16] These approaches offer precise manufacturing but require complex apparatuses and complicated series of processing steps.[17]

"Bottom-up" approaches, such as self-assembly of colloidal crystals or polymers, are rapid and relatively inexpensive techniques to prepare photonic crystals under mild processing conditions.[18] One limitation of colloidal templating is the low refractive index contrast for typical colloidal materials, and infilling with inorganic materials is often required to achieve photonic properties, increasing costs and the number of fabrication steps.[19] Furthermore, colloidal assembly is generally limited to face-centered cubic geometries.

Modern polymerization techniques that allow for control of molecular weights and chain architectures have made polymeric multilayer films attractive in photonic crystal applications.[20] These soft materials have controllable compositions, structures, and mechanical properties,[21] and they are flexible and easily molded to meet geometric specifications. While the refractive index contrast between polymer-based components is relatively small,[22] this can be compensated for by forming structures with a large number of layers (Equation 3) or by blending with high-index components (Section 4.3). As described below, polymeric materials are able to access a wide range of 1D, 2D, and 3D periodic dielectric structures, which can be controlled by the composition and architecture of these materials.

2. Properties of Bottlebrush Copolymers

Polymers are amenable to use in a wide range of applications due to their highly varied and tunable properties. The physical attributes of polymers can be controlled by monomer selection and macromolecular structure (i.e., molecular weight, shape, and branching). In the following Section, the self-assembly of diblock copolymers will be discussed, with an emphasis on differences between linear and brush polymer architectures.

2.1. General Principles of Block Copolymer Self-Assembly

Block copolymers (BCPs) consist of two or more chemically distinct polymers (blocks) that are sequentially incorporated in the same polymer chain, and the self-assembly of these materials constitutes a powerful tool for the synthesis of nanostructured materials.[23] In general, the phase behavior of an AB diblock copolymer (**Figure 1**) is dictated by: (1) the volume fractions of the A and B blocks (f_A and f_B, with $f_A + f_B = 1$), (2) the total degree of polymerization ($N = N_A + N_B$), and (3) the Flory-Huggins parameter, χ_{AB}.[23] The χ-parameter describes the penalty for A/B mixing due to the incompatibility of the A and B segments. At sufficiently high segregation strengths (χN), microphase separation occurs. The particular ordered phase that is favored is dictated by a balance between the enthalpic drive to minimize the unfavorable A/B segment contacts, while simultaneously maximizing the conformational entropy of polymer chains. Symmetric diblock copolymers favor lamellar morphologies, while asymmetric volume fractions lead to cylindrical, gyroid, or spherical ordered phases.[22, 24]

Typically, linear block copolymers (LBCPs) with molecular weights ranging from 10–100 kDa can be readily prepared, which assemble to structures with domain sizes from 10–40 nm.[25] However, it remains challenging to access the larger domain spacings necessary to reflect

visible light (>70 nm).[26] In addition to the synthetic difficulty of preparing very high molecular weight linear copolymers,[27] these materials are often highly entangled in the melt, which inhibits their ability to assemble into long-range ordered structures.[25, 28] When cast from solution, high molecular weight LBCPs can form well-ordered structures with periodicities large enough to reflect visible light;[27, 29] however, these processing methods can be slow, and careful optimization of conditions such as solvent and temperature is required to create uniform and reproducible assemblies.

2.2. Bottlebrush Block Copolymer Self-Assembly

Brush polymers, also called bottlebrushes, feature polymeric side chains grafted to a linear backbone (Figure 1, bottom). The high branch-to-backbone ratio in these systems causes bottlebrush polymers to display different conformational behavior than linear polymers.[30] Bottlebrush polymers adopt worm-like, cylindrical conformations that are relatively extended.[31]

The bottlebrush architecture is beneficial in facilitating self-assembly to structures with large domain sizes. Rheological studies have demonstrated that brush polymers with side-chain lengths below entanglement molecular weight do not entangle, even in the ultrahigh molecular weight regime of up to thousands of kilodaltons (over an order of magnitude higher than the entanglement molecular weight of most linear polymers).[32] This has been attributed to backbone elongation due to the steric congestion between adjacent side chains. Entanglement presents a kinetic barrier to reorganization during self-assembly, so architectures that minimize entanglement may display more rapid self-assembly.

The faster ordering kinetics of bottlebrush block copolymers have been measured by in situ small-angle X-ray scattering (SAXS). Russell and co-workers have studied self-assembly of symmetric brush block copolymers (BBCPs) with polylactide (PLA) and polystyrene (PS) side chains ($M_n \sim$ 2.4 kDa for both PLA and PS).[33] Formation of a lamellar phase was observed within 5 minutes for a 118 kDa sample annealed at 130 °C. A higher molecular weight sample (529 kDa) required 1 hour to assemble at the same temperature. In contrast, a 50 kDa linear PS-*b*-PLA diblock did not display well-developed order after 24 hours of thermal annealing, suggesting that the bottlebrush architecture displays significantly faster ordering compared to linear systems.

The scaling of domain spacing with degree of polymerization also differs between linear and brush block copolymers. For strongly segregated LBCPs, domain spacing, d, is determined by the scaling relationship $d \sim N^{2/3}\chi^{1/6}$.[23] The scaling exponent for BBCPs has only been determined in a few studies,[28, 33-34] and this relationship is not well understood. Gu et al. compared two series of symmetric BBCPs with PS and PLA side chains.[33] For the first series, relatively short 2.4 kDa side chains were featured on both blocks, whereas the second series had blocks with ~4.4 kDa side chains. Domains spacings, as measured by SAXS, were fit to a power law $d \sim N^{\alpha}$, and the samples with lower molecular weight side chains were observed to exhibit a larger scaling exponent ($\alpha = 0.91$) than those for the other series ($\alpha = 0.84$). The relatively large scaling exponents for these series (compared to LBCPs) were attributed to a more extended conformation of BBCPs relative to linear systems.[33] However, recent work by Dalsin et al. for BBCPs featuring PS and atactic polypropylene (aPP) side chains indicates that the scaling exponent depends on backbone length, ranging from $\alpha \approx 0.3$ at small backbone lengths to $\alpha \approx 0.9$ as N increases.[34] This work suggests that BBCPs transition from being starlike to brushlike as the backbone length increases relative to the side chain length; however, there can be considerable bending of BBCPs, even with long backbones.

For all block copolymer architectures, relative volume fractions crucially shape self-assembly. For LBCPs, only the length of the two segments can modify the composition, whereas BBCP assembly is influenced by both the backbone and brush side chain lengths. Rzayev and co-workers have demonstrated that asymmetric BBCPs, which contained symmetrical backbone blocks, but asymmetric side chain lengths, assembled to cylindrical structures with diameters as large as 55 nm (**Figure 2**).[35] Complementary work from our group has shown that non-lamellar morphologies are accessible by utilizing BBCPs with asymmetric backbone block lengths.[36] These studies present two strategies to alter the volume fractions and therefore influence the resulting morphology of a brush copolymer: the backbone block lengths or the side chain molecular weights can be adjusted.

In summary, BBCPs display unique rheological properties and rapid ordering kinetics as a consequence of the densely grafted molecular architecture. These are beneficial in the self-assembly of structures with large domain sizes and long-range order, which are requirements for photonic crystal applications. The following Section describes specific examples of BBCP photonic materials.

3. Bottlebrush Block Copolymer Assembly to Photonic Crystals

3.1. Strategies to Prepare Bottlebrush Polymers

There are three general methods to prepare brush polymers, called the "grafting-to," "grafting-from," and "grafting-through" approaches (**Figure 3**).[37] The grafting-to method

involves covalent attachment of monotelechelic (functionalized on one chain end) polymer chains to a functional backbone. Common reactions to attach polymeric side chains include nucleophilic substitution and copper(I)-catalyzed azide–alkyne "click" coupling reactions.[38] This approach allows for good control of backbone and side chain dispersities ($Đ$); however, the grafting density is often low (<60%), as coupling between two macromolecular species at tightly spaced intervals can be challenging.[37a] The grafting-to approach has not been widely used due to this limitation.

The grafting-from method directly grows the polymeric side chains from initiation sites distributed along the polymeric backbone. This approach is highly modular, which allows for generation of a variety of bottlebrushes with different compositions or molecular weights from a single macroinitiator. There is good control of backbone dispersity using this approach; however, grafting density and side chain dispersity are only moderately controlled, as there can be steric difficulties with initiation and side chain polymer growth.[38] Preparation of copolymers using a grafting-from technique can also be synthetically challenging; multiple protection/deprotection steps may be necessary for sequential side chain polymerizations.[37a]

Lastly, the grafting-through method involves the direct polymerization of monotelechelic polymers, also referred to as "macromonomers".[39] Similar to grafting-to synthesis, the grafting-through method has the advantage that the side chains can be characterized prior to bottlebrush synthesis. This route generates materials with uniform side chain molecular weight and grafting density, as every backbone monomer contains a side chain. One drawback is that steric hindrance at the propagating poly macromonomer chain end can be a problem; however, appropriate design of the macromonomer and catalyst can overcome this challenge.

Ultimately, the choice of synthetic strategy depends upon the requirements of the application of interest. If uniform grafting density is not critical, the grafting-to or -from methods are potentially preferable, as they are highly modular. If high grafting density and uniform side chain length are required, the grafting-through method is superior.

3.2. Synthesis and Self-Assembly of Brush Block Copolymer Photonic Crystals

Runge and Bowden provided the first demonstration that block copolymers with at least one grafted block can have advantages accessing domains large enough to reflect visible light.[40] Sequential ruthenium-catalyzed ring-opening metathesis polymerization (ROMP) of oxanorbornene monomers afforded a diblock copolymer in which one block is decorated with atom transfer radical polymerization (ATRP) initiator sites and the other block bears hexanoate groups (**Figure 4**). Following hydrogenation of the backbone, polystyrene arms were grown by copper-catalyzed ATRP from the initiation sites. This procedure afforded high molecular weight copolymers (M_n = 730–6,400 kDa) with moderately controlled molecular weight distributions ($Đ$ = 1.17–1.44). These polymers contain highly asymmetric branch lengths, as only one of the blocks is decorated with polymeric side chains. These asymmetric copolymers are termed brush-coil diblocks or "comb block polymers."

Thin films of polystyrene/hexanoate copolymers were prepared by controlled evaporation from dichloromethane, followed by annealing for 24 hours at 100 °C. A range of morphologies was observed by SEM, including lamellae, cylinders, and spheres, depending on the volume fraction of the polystyrene component (**Table 1**). Increasing asymmetry in the volume fractions of the two blocks by varying the relative backbone length (expressed as the mol% of polystyrene in Table 1) leads to preferential formation of cylindrical or spherical phases. For a given morphology, higher molecular weight samples have larger domain sizes.

Photonic properties were noted for one sample (M_n = 2030 kDa, Entry 4 in Table 1), which appeared blue after complete evaporation of dichloromethane. The wavelength of maximum reflectance (λ_{max}) could be shifted from 385 nm to 445 nm by exposure to dichloromethane vapor. This shift to longer wavelength (corresponding to a color change from blue to green) is due to solvent swelling of domain sizes. Interestingly, this photonic crystal corresponds to a sample with spherical morphology; in contrast, all other BBCP-based photonic crystals discussed in this Feature Article have lamellar structures. Access to the spherical morphology may be enabled by the unique brush-coil architecture.

Rzayev has also utilized a grafting-from method to prepare polylactide/polystyrene BBCP photonic crystals (**Figure 5**).[25] The backbone was synthesized by sequential reversible addition-fragmentation chain-transfer (RAFT) polymerization of solketal methacrylate and 2-(bromoisobutyryl)ethyl methacrylate. Polystyrene branches were grown from the bromide-containing initiator sites by copper-catalyzed ATRP. Subsequently, the ketal groups were hydrolyzed, and DBU-catalyzed ring-opening polymerization of lactide was performed from the resulting hydroxyl groups. NMR and GPC analysis indicated that high initiation efficiency was achieved during styrene polymerization (>90%), whereas slightly lower efficiency was observed for lactide polymerization (70–90%).

Samples were melt-pressed at 170 °C for 16 hours, and a high molecular weight sample (M_n = 2400 kDa, f_{PLA} = 0.37) was observed to reflect blue light (**Figure 6**). Morphologies were assigned by ultra-small-angle X-ray scattering (USAXS) and verified by scanning electron microscopy (SEM) (Figure 6). The relative block lengths along the backbone were varied to assess the impact of compositional asymmetry on morphology. Lamellar morphologies were

exclusively observed, even for highly asymmetric BBCPs (f_{PLA} = 0.3). For the blue sample shown in Figure 6, (M_n = 2400 kDa, f_{PLA} = 0.37), a domain spacing of 153 nm was obtained from USAXS, and thicknesses of the PLA and PS layers (d_{PLA} = 57 nm and d_{PS} = 96 nm) were calculated from the domain spacing and volume fraction of the BBCP. Domain spacing increased linearly with backbone length, which was attributed to an extended conformation. In comparison, typical coil-coil LBCPs are expected to display cylindrical or spherical morphologies at this volume ratio[22] and typically exhibit domain spacings that scale by $MW^{2/3}$.[23, 41]

Ring-opening metathesis polymerization (ROMP) is a powerful approach to grafting-through synthesis of bottlebrush polymers. Ruthenium-catalyzed ROMP has been demonstrated for a range of macromonomers, taking advantage of the ring strain of the norbornene monomer, high activity of ruthenium metathesis catalysts, and the stability of the propagating species to enable the synthesis of well-defined bottlebrush polymers.[42] These catalysts exhibit excellent functional group and steric tolerance, which are necessary to polymerize macromonomers with diverse functionalities and side chain lengths.

Xia et al. investigated grafting-through polymerization of polylactide (PLA) and poly(*n*-butyl acrylate) (P*n*BA) macromonomers by ROMP (M_n = 4.7 and 4.0 kDa for PLA and P*n*BA macromonomers, respectively) (**Figure 7**).[39b] Living ROMP characteristics were observed, and molecular weights could be controlled by the macromonomer-to-ruthenium molar ratio. Due to similar polymerization rates, brush random polymers *g*-[PLA-*ran*-P*n*BA] could be prepared by initiating a mixture of the two macromonomers. BBCPs *g*-[PLA-*b*-P*n*BA] were prepared by

sequential addition of macromonomers. Samples with high molecular weights (M_n = 450–1880 kDa) and narrow dispersities ($Đ$ = 1.07–1.10) were prepared by this method.

Domain spacings were determined by SAXS for random and block copolymers that were thermally annealed at 100 °C for 12 hours. Lamellar morphologies were exclusively observed. For random copolymers, domain spacings determined by SAXS were observed to be independent of backbone length (14.3 ± 0.3 nm), which was in good agreement with measurements of lamellar thicknesses of 17 to 20 nm by atomic force microscopy (AFM). The lack of dependence of lamellar spacing on backbone length suggests that these samples assemble by segregation of the PLA and P*n*BA side chains to opposite sides of the polynorbornene backbone (**Figure 8**). A much larger *d*-spacing of 116 nm was measured for a symmetric block copolymer *g*-[PLA_{100}-*b*-P*n*BA_{100}] (M_n = 980 kDa). Furthermore, a higher molecular weight copolymer *g*-[PLA_{200}-*b*-P*n*BA_{200}] (M_n = 1770 kDa) reflected green light upon slow evaporation of THF. The large lamellar spacings of the block copolymers suggest that the backbone is oriented orthogonal to the lamellae for this architecture. This work demonstrated that polymer sequence (i.e., random or block) can control domain spacing in brush copolymer nanostructures.

Sveinbjörnsson et al. have investigated the effects of BBCP molecular weight and assembly method on photonic properties. PS and PLA macromonomers were synthesized from *exo*-norbornene-functionalized initiators by ATRP and ring-opening polymerization, respectively. Symmetric BBCPs were prepared by sequential ROMP of these macromonomers,

producing samples with extremely high molecular weights (M_n = 1080–6440 kDa) and acceptable molecular weight distributions ($Đ$ = 1.07–1.58).

A number of methods to produce photonic films were compared, including controlled evaporation from DCM or THF and thermal annealing. The film preparation method had a dramatic effect on photonic properties. For one BBCP sample (M_n = 2940 kDa), films cast from DCM, THF, or that were thermally annealed appeared blue, green, or red, respectively (**Figure 9**). SEM images were obtained to compare morphologies for these samples. Films cast from DCM appeared as highly disordered lamellae (Figure 9B), while evaporation from THF afforded larger and better-ordered lamellar domains (Figure 9C). This solvent effect may be in part due to different kinetics of evaporation or quality of solvent;[43] however, because these samples are not long-range ordered, differences in grain size or the orientation of lamellae may also contribute to the reflectance properties of these samples. Thermal annealing resulted in the greatest thickening of lamellae (Figure 9D,E), consistent with the observation of the longest wavelength reflections by this preparation method.

Films of a 2940 kDa BBCP prepared by controlled evaporation exhibited a maximum wavelength of reflectance (λ_{max}) of 540 nm. Impressively, direct thermal annealing of a higher molecular weight sample (M_n = 6640 kDa) under compression produced a film that reflected at near-infrared (NIR) wavelengths (λ_{max} = 1311 nm).[7] At the time, this was an unprecedented wavelength regime for unswelled polymer-based photonic crystals. However, the samples in this series that reflect wavelengths of >1000 nm have low reflectivities and large bandwidths, indicating poor ordering of the highest molecular weight samples, an ongoing challenge for producing well-ordered NIR-reflecting BBCPs. The reflectance maximum (and therefore,

domain spacing) was a linear function of molecular weight for all self-assembly techniques analyzed, which was attributed to a greater degree of backbone extension for brush polymers relative to linear materials. The angle-dependent reflectance spectra were measured for a well-ordered sample (M_n = 1530 kDa), and good agreement of the angular frequency response was observed between experiment and transfer matrix simulations.

Development of methods to assemble photonic materials under ambient conditions could enable widespread applications. To facilitate self-assembly, Miyake et al. developed isocyanate-based macromonomers,[44] as poly(isocyanates) are known to adopt rigid, helical structures.[45] The rigid structure of poly(isocyanates) has also been exploited in the context of LBCPs, and poly(hexyl isocyanate-*b*-styrene) rod-coil block copolymers have demonstrated periods as large as 1000 nm.[46] For BBCPs, use of rigid side chains, rather than random-coil side chains, can reduce entanglement and increase main chain elongation to facilitate self-assembly.[47] BBCPs featuring poly(hexyl isocyanate) and poly(4-phenyl butyl isocyanate) side chains were prepared by graft-through ROMP of corresponding macromonomers. High molecular weight materials were prepared (M_w = 1512–7119 kDa) with low molecular weight distributions ($Đ$ = 1.08–1.39) (**Figure 10**).

Film preparation methods were compared, including controlled evaporation from DCM, THF, $CHCl_3$, and toluene. There was no solvent effect on self-assembly, as determined by comparing λ_{max} values for the cast films. This is in contrast to previous observations for PS/PLA BBCPs (Figure 9).[7] Samples with molecular weights (M_w) of 1512, 2918, and 4167 kDa appeared violet, green, and red, consistent with the primary reflectance peaks observed for these samples (λ_{max} = 334, 511, and 664 nm, respectively, **Figure 11**). SEM images confirmed

the lamellar morphologies of these samples. Higher molecular weight BBCPs (5319 and 7119 kDa) exhibited broad reflectance peaks centered at 801 nm and 1120 nm, and SEM analysis indicated that these samples displayed unordered morphologies and lacked well-defined domains. This method of using stiff isocyanate-based side chains provided a significant improvement in the wavelengths of reflectance accessible by controlled evaporation under ambient conditions.

There are three potential causes of dispersity in the BBCP architecture: the polymeric main chain, and the two polymeric brush components. Although dispersity is known to have a neutral or beneficial effect on enhancing the self-assembly of LBCPs,[48] dispersity could potentially lead to non-uniform assembly, causing broad reflectance bandwidths. To reduce overall dispersity in BBCPs, Piunova et al. investigated the use of dendronized block copolymers to prepare uniform polymer-based photonic crystals.[49] Dendritic polymers exhibit low chain entanglement due to steric repulsion between pendant substituents, making them promising components to promote rapid self-assembly. Additionally, these materials require lower total molecular weights than BBCP systems with polymeric side chains, which lowers viscosity while still achieving similar degrees of sterically induced backbone extension.

Discrete norbornene wedge-type monomers featured either decyl or benzyl ether substituents radiating from a central aryl core (**Figure 12**). Dendronized block copolymers with high molecular weights (M_w = 480–3340 kDa) and low polydispersities ($Đ$ = 1.05–1.23) were prepared by ROMP. Samples with molecular weights ranging from 480 to 1390 kDa reflected in the visible to NIR (λ_{max} = 330–888 nm) upon controlled evaporation from DCM (**Figure 13**). Higher molecular weight dendronized block copolymer samples did not assemble to ordered

structures or reflect light. This was attributed to reduced main chain rigidity for dendronized samples leading to chain entanglement that hampers assembly.

A notable result from these studies was that dendronized block copolymers possessed significantly narrower bandwidths in the visible range compared to previous BBCPs. This was quantified by comparing gap–midgap ratios (GMRs), calculated as the full width at half λ_{max} divided by λ_{max} (GMR = $\Delta\lambda$ / λ_{max}) for dendronized and poly(isocyanate) block copolymers. GMR values for dendritic samples (9–18%) were significantly smaller than those featuring poly(isocyanate) brushes (GMR = 17–27%). Low GMRs imply more uniform domain sizes, which was attributed to the elimination of side group dispersity for the materials featuring discrete monomers. Annealing samples for 24 h at 100 °C caused red-shifting of λ_{max} values by 75–335 nm, accompanied by bandwidth broadening and decreased reflectance intensity (Figure 13). This behavior may be due to uneven thickening of lamellae throughout these films during thermal annealing.

4. Strategies Toward Tuning of Optical Properties

The grafting-through method employing ruthenium-catalyzed ROMP represents a significant advancement toward the synthesis of high molecular weight BBCPs with low molecular weight distributions. However, synthetic challenges remain that hinder the design and processability of BBCPs and their potential use in photonic applications. Such challenges include increasing dispersity at ultra-high molecular weights, required optimization of

polymerization conditions for each BBCP, and the incorporation of functional groups not compatible with ROMP catalysts. A number of strategies have been developed to post-synthetically tune the photonic properties of LBCPs,[50] but it could not be assumed that these would be similarly effective for BBCPs, which exhibit comparatively rigid structures due to densely grafted side chains. However, recent studies of polymer blends have suggested that in some cases, tuning BBCP optical properties does not require the synthesis of discrete high molecular weight BBCPs to reflect specific wavelengths of light. The following Section describes different blending strategies to affect the photonic properties of BBCPs, including blends with linear polymers, brush polymers, and nanoparticles.

4.1. Blends with Linear Homopolymers

Macfarlane et al. reported blending of PS/PLA BBCPs with linear homopolymer (HP) additives.[51] A symmetric BBCP (M_n = 987 kDa) was blended with PS and PLA HPs (PS:PLA = 1:1) of similar molecular weights as the side chains (≈3 kDa) (**Figure 14**). After thermal annealing at 140 °C overnight, the self-assembled blends exhibited a positive linear correlation between lamellar domain spacing and the HP:BBCP weight ratio (**Figure 15A**). Higher molecular weight BBCPs could accommodate higher HP loadings (up to a HP:BBCP weight ratio of 3:1), and arrays were observed to swell up to 180% of the domain spacings of the unblended BBCPs, allowing for reflection at long wavelengths in the telecommunications regime (λ = 1200–1650 nm) (**Figure 15B**). Self-consistent field theory demonstrated that the HPs are incorporated into the lamellar blocks that contain brushes of the same composition. The HPs are evenly distributed throughout the BBCP blocks, with only slightly higher amounts of HPs at the block interfaces and the centers of the lamellae.

The highly ordered nature of blends with intermediate HP levels was attributed to the tendency of low-molecular-weight HPs to increase the homogeneity of lamellar packing, reducing any scattering from diffuse interfaces. Specifically, GMR values ($\Delta\lambda$ / λ_{max}) narrow upon addition of HP additives. For one BBCP sample (M_n = 987 kDa), the GMR decreased from 24% to 20% upon addition of 65 wt% of HPs. Blending low molecular weight HP additives provided a simple method for generating an array of PCs with different optical properties and large domain spacings, without necessitating the synthesis of individual high molecular weight BBCPs. Furthermore, the addition of HPs bearing functional groups that inhibit ROMP provided a convenient route to introduce these functionalities into well-ordered PCs. This study was the first to generate PCs by blending BBCPs with copolymers bearing various functional groups. Gaining a stronger understanding of blending effects on the refractive index and reflectivity, effective χ, and stability of polymer films requires further study.

4.2. Blends with Brush Block Copolymers

Another facile approach to rapidly tune the photonic band gap is the blending of block copolymers of two different molecular weights. The self-assembly of this type of polymer blend has been investigated for LBCPs,[52] but only recently have similar polymer blends been investigated for the comparatively rigid BBCPs. Miyake et al. reported that poly(isocyanate) BBCPs could exhibit reflections between 334 and 1120 nm by altering backbone chain length (Figure 10 and 11).[44] In a later report, Miyake et al. demonstrated that by simply blending two poly(isocyanate)-based BBCPs of different molecular weights (M_w = 1512 and 4167 kDa) in different ratios, a spectrum of PCs reflecting from visible to NIR light could be quickly generated by controlled evaporation from DCM (**Figure 16**A).[53] The peak wavelength of reflectance (λ_{max})

is highly predictable based on a linear correlation with the blend ratio (**Figure 16**B), indicating the convenience of this strategy toward practical application. Furthermore, SEM images confirmed the formation of lamellar morphologies of both the polymer blends and the parent BBCPs (**Figure 16**C), suggesting that despite the rigid architecture of the poly(isocyanate) BBCPs, blends of these polymers are able to assemble to uniform, layered structures. Although this result has not yet been observed for other BBCP architectures, this study lays the groundwork for tailoring BBCP photonic crystals to specified desired optical properties by simply blending polymers with different molecular weights.

4.3. Brush Block Copolymer Nanocomposites

BBCPs exhibit reduced chain entanglement[32a, 39b] compared to linear analogues and rapidly self-assemble to nanostructures with large domain spacing. These characteristics make BBCPs favorable candidates as platforms for templating nanoparticles (NPs) into ordered domains, a strategy previously utilized to tune the optical properties of LBCPs.[54] Watkins and co-workers have demonstrated that BBCPs can accommodate high NP loading concentrations by designing strong, preferential interactions between NPs and one block of a BBCP. These interactions prevent NP aggregation and promote uniform distribution of the NPs in one domain.[55]

Song et al. have investigated the incorporation of gold NPs into polystyrene/poly(ethylene oxide) (PS-*b*-PEO) BBCPs (**Figure 17**).[55c] Gold NPs with ≈2 nm core diameter supported by 4-mercaptophenol ligands were utilized, as strong hydrogen-bond interactions with these ligands allow for the selective incorporation of gold NPs in the PEO domains of these BBCPs. Composite films with NP loadings as high as 67.2 wt% (Au% = 48.4 wt%) could be prepared by drop casting THF solutions of BBCPs and gold NPs. By varying the

NP concentration in the PEO layer or by increasing BBCP molecular weight, lamellar domain spacings (as determined by SAXS and TEM) could be controlled from 120 to 260 nm. These structures resulted in photonic band gaps that were tunable from the visible to the NIR (λ_{max} = 458–1010 nm) (**Figure 18**A **and Figure 18**B). For a film containing 58.3 wt% of gold NPs, thermal annealing at 120 °C for 8 hours led to a red shift in λ_{max} from 598 to 736 nm (**Figure 18**C). Change in the reflectance occurred with lengthened annealing times (**Figure 18**D), which was attributed to an increase in the gold NP size.[56] While manipulation of the gold NP/PEO layer allowed for reflection from visible to NIR light and increased refractive indices, the gold NPs absorb visible light, which may limit applications of these materials as coatings.

The problem of low reflectance was addressed by the Watkins group in a later report, using blends of functionalized zirconium oxide (ZrO_2) NPs, which are transparent to visible light, and P*t*BA-*b*-PEO (P*t*BA = poly(*tert*-butyl acrylate)) BBCPs to form photonic nanocomposites with high refractive index contrast (Δn).[55b] The refractive index of the NP/PEO layer increased linearly with NP concentration (**Figure 19**A). Although for typical polymeric PCs $\Delta n \leq 0.1$, the ZrO_2 NP/BBCP nanocomposites reached refractive index contrasts up to $\Delta n > 0.27$ (Figure 19B). These high Δn values can improve performance of photonic coatings by reducing the number of layers necessary to achieve high reflectivity (Figure 19C and Figure 19D and Equation 3). Furthermore, photoluminescence studies showing multiphoton excitation emission suggest that related hybrid materials containing CdSe NPs can be useful in nonlinear optical applications.[55a] The generation of well-ordered NP arrays via BBCP self-assembly lends an abundance of new applications and tuning capabilities for photonic hybrid materials.

Recently, Song et al. have reported symmetrical P*t*BA-*b*-PEO BBCPs that can self-assemble to architectures with long-range order.[57] A highly oriented lamellar morphology with a domain spacing of 97 nm was observed by SAXS after thermally annealing a 1850 kDa sample at 110 °C for 5 min. Layer orientations throughout a polymer sample were measured by continuous SAXS scan measurements. Grain sizes that correspond to an area of 5.40 mm^2 and a volume of 3.56 mm^3 were observed, which are significantly larger than those observed for LBCPs. Gold NPs (~2 nm core diameter supported by 4-mercaptophenol ligands) were selectively incorporated into the PEO domains of the P*t*BA-*b*-PEO structure. Upon increasing gold NP loading from 0 to 60 wt% (29 vol%), the domain spacing increased from 97 to 125 nm. Long-range ordering was maintained upon incorporation of gold NPs. This work provides a straightforward method to prepare highly ordered structures with millimeter-scale grain sizes both in the presence and absence of nanoparticle additives.

5. Conclusion and Outlook

Brush block copolymers (BBCPs) have been demonstrated as promising materials for the bottom-up synthesis of photonic crystals. The reduced entanglement, ability to access large domain spacings, and superior self-assembly kinetics associated with this architecture motivate the use of these materials. Through control of side chain rigidity, exceptionally fast self-assembly has been realized. Fabrication of BBCP thin films is now feasible by controlled solvent evaporation under ambient conditions, which enables applications that necessitate inexpensive and rapid fabrication.

The advancements in our understanding of BBCPs also raise new questions and suggest further research opportunities. Additional fundamental studies of BBCP self-assembly are needed to understand the thermodynamics of ordering and how it differs from LBCPs.[37a] The effect of specific bottlebrush structural parameters, such as branch length, backbone length, or

grafting density, on assembled structure is not well understood. In several reports of BBCP photonic crystals, a linear relationship between λ_{max} and molecular weight is reported, which was attributed to highly extended conformations of these materials.[7, 25, 44, 49] However, recent work by Dalsin et al. (Section 2.2) has demonstrated that the scaling of domain spacing depends on the length of the backbone relative to that of the side chains, reaching a maximum value of $\alpha \approx 0.9$ for high N samples.[34] Furthermore, self-consistent field theory suggests that BBCPs may be more flexible than previously assumed, and there may be considerable bending of the backbones in the lamellar morphology, particularly near the center of the domains.[34] While the majority of reported BBCPs feature lamellar morphologies, limited examples of cylindrical,[35, 40a] spherical,[40a] and gyroid[58] phases have been observed by manipulation of macromonomer design. This motivates further investigations of the unique phase behavior of the bottlebrush block copolymer architecture with the goal of creating predictive models for self-assembly.

Continued attention should be paid to determining the factors that control the uniformity of self-assembly for BBCPs. In particular, achieving well-ordered BBCPs that reflect NIR light (λ = 750–1500 nm) remains challenging. Both slow diffusion rates and relatively high dispersities for ultra-high molecular weight BBCPs are challenges to producing well-ordered NIR-reflecting photonic crystals. Although the peak wavelength of reflection (λ_{max}) in BBCPs can be readily tuned by backbone degree of polymerization, the bandwidths of these materials are somewhat large and broaden with increasing λ_{max}.[49] Better control of bandwidths in these photonic crystals is desirable for some applications.[6] Furthermore, for practical fabrication of BBCP photonic crystals, alternative self-assembly methods may be required. In particular, shear alignment techniques may be beneficial in fabricating paintable BBCP photonic coatings. Shear alignment of colloidal materials and linear block copolymers is well known;[59] however, to our knowledge, no reports utilize this technique to prepare BBCP films.

Responsive photonic crystals[19a, 19c, 60] represent another avenue of research in which BBCPs may be advantageous. Reversible color changes in response to a physical or chemical stimulus are desired in applications as sensors, indicators, or color displays.[61] To borrow concepts from other classes of chromotropic materials, it may be possible to prepare BBCP photonic crystals that are sensitive to temperature,[62] strain,[63] ionic strength and pH,[64] or the presence of an electric field.[65] The development of "switching" mechanisms for these structures would provide new routes to responsive materials.

In conclusion, BBCPs have been successfully applied to improve the viability of polymer-based photonic crystals as practical optical elements. This represents an exciting field with both interesting fundamental and technological facets. Significant synthetic effort over the last decade has improved our understanding of the design, fabrication, and tuning of these materials. Opportunities exist for further development of BBCP photonic crystals both through optimizing existing materials and designing new systems and self-assembly methods.

Acknowledgements: We would like to acknowledge the many co-workers over the years who have contributed to the research described above. The U.S. National Science Foundation (CHE-1048404), U.S. Department of Energy (DE-SC0001293), and a Dow Resnick Bridge Award funded aspects of our research in this area. A.L.L.-M. thanks the Resnick Sustainability Institute at Caltech for fellowship support. We thank Alice B. Chang for insightful discussions during the preparation of this manuscript.

Received:; Revised:; Published online: XX, XXXX; DOI: 10.1002/ marc.201700058

Keywords: photonic crystals, bottlebrush, block copolymers, self-assembly, structural color

Allegra L. Liberman-Martin received her B.A. degree from Scripps College in 2010. She completed her Ph.D. in 2015 with Profs. T. Don Tilley and Robert G. Bergman at the University of California, Berkeley. Allegra is currently a Resnick Sustainability Institute Postdoctoral Fellow working with Prof. Robert H. Grubbs at the California Institute of Technology. Her research focuses on side chain design in bottlebrush copolymers with photonic applications.

Crystal K. Chu completed her B.S. in Chemistry from the University of California, Berkeley in 2012. She then joined the graduate program in chemistry at the California Institute of Technology, where she is currently a graduate student in the laboratory of Professor Robert H. Grubbs. Her current research interests include organic, organometallic, and polymer chemistry.

Robert H. Grubbs is currently the Victor and Elizabeth Atkins Professor of Chemistry at the California Institute of Technology, where he has been a faculty member since 1978. Before moving to Caltech, Bob was at Michigan State University from 1969 to 1978, where he achieved the rank of Associate Professor. He received his B.S. and M.S. degrees from the University of Florida and his Ph.D. from Columbia University. His research examines the design of catalysts for use in organic and polymer synthesis.

Application of Bottlebrush Block Copolymers as Photonic Crystals

Allegra L. Liberman-Martin, Crystal K. Chu, Robert H. Grubbs*

Brush block copolymers have emerged as promising components in the bottom-up synthesis of photonic crystals from common organic chemical feedstocks. This polymer architecture permits fabrication of photonic crystal films under ambient conditions driven by self-assembly. Photonic properties can be controlled by the backbone length of the brush block copolymer or by utilizing blending techniques.

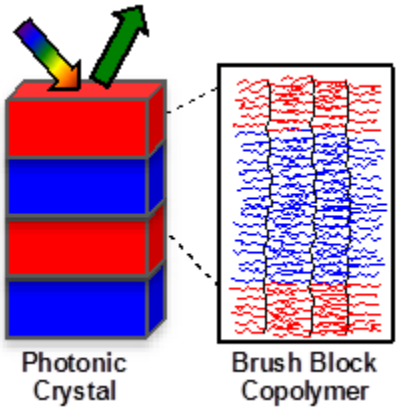

<comp>TYPESETTER: Please delete the final page number from each reference, so that only the first page number is provided.</comp>

[1] a) M. Qiu, M. Mulot, M. Swillo, S. Anand, B. Jaskorzynska, A. Karlsson, M. Kamp, A. Forchel, *Appl. Phys. Lett.* **2003**, *83*, 5121-5123; b) Y. Mahmoud, G. Bassou, A. Taalbi, Z. M. Chekroun, *Optics Communications* **2012**, *285*, 368-372.

[2] M. Malekmohammad, M. Soltanolkotabi, A. Erfanian, R. Asadi, S. Bagheri, M. Zahedinejad, M. Khaje, M. H. Naderi, *J. Euro. Opt. Soc. Rapid Public.* **2012**, *7*, 12008.

[3] a) H. Ding, C. Liu, H. Gu, Y. Zhao, B. Wang, Z. Gu, *ACS Photonics* **2014**, *1*, 121-126; b) H. Ding, C. Liu, B. Ye, F. Fu, H. Wang, Y. Zhao, Z. Gu, *ACS Appl. Mater. Interfaces* **2016**, *8*, 6796-6801.

[4] J. Rosenberg, R. V. Shenoi, S. Krishna, O. Painter, *Optics Express* **2010**, *18*, 3672-3686.

[5] J. D. Joannopoulos, S. G. Johnson, J. N. Winn, R. D. Meade, *Photonic Crystals: Molding the Flow of Light*, 2nd ed., Princeton University Press, Princeton, NJ, **2008**.

[6] Y. Wang, D. Chen, G. Zhang, J. Wang, S. Tao, *Optics Commun.* **2016**, *363*, 13-20.

[7] B. R. Sveinbjörnsson, R. A. Weitekamp, G. M. Miyake, Y. Xia, H. A. Atwater, R. H. Grubbs, *Proc. Natl. Acad. Sci. USA* **2012**, *109*, 14332-14336.

[8] M. Maldovan, E. L. Thomas, *Periodic Materials and Interference Lithography*, Wiley-VCH Publishers, Weinheim, **2009**.

[9] E. Yablonovitch, *J. Phys. Condens. Matter* **1993**, *5*, 2443-2460.

[10] C. Paquet, E. Kumacheva, *Materials Today* **2008**, *11*, 48-56.

[11] J. H. Moon, S. Yang, *Chem. Rev.* **2010**, *110*, 547-574.

[12] J.-H. Lee, C. Y. Koh, J. P. Singer, S.-J. Jeon, M. Maldovan, O. Stein, E. L. Thomas, *Adv. Mater.* **2014**, *26*, 532-569.

[13] S. Y. Lin, J. G. Fleming, D. L. Hetherington, B. K. Smith, R. Biswas, K. M. Ho, M. M. Sigalas, W. Zubrzycki, S. R. Kurtz, J. Bur, *Nature* **1998**, *394*, 251-253.

[14] M. Campbell, D. N. Sharp, M. T. Harrison, R. G. Denning, A. J. Turberfield, *Nature* **2000**, *404*, 53-56.

[15] S. Jeon, J.-U. Park, R. Cirelli, S. Yang, C. E. Heitzman, P. V. Braun, P. J. A. Kenis, J. A. Rogers, *Proc. Natl. Acad. Sci. USA* **2004**, *101*, 12428-12433.

[16] H. Masuda, M. Ohya, H. Asoh, M. Nakao, M. Nohtomi, T. Tamamura, *Jpn. J. Appl. Phys.* **1999**, *38*, 1403-1405.

[17] J. A. Liddle, G. M. Gallatin, *ACS Nano* **2016**, *10*, 2995-3014.

[18] J. F. Galisteo-López, M. Ibisate, R. Sapienza, L. S. Froufe-Pérez, Á. Blanco, C. López, *Adv. Mater.* **2011**, *23*, 30-69.

[19] a) J. Ge, Y. Yin, *Angew. Chem. Int. Ed.* **2011**, *50*, 1492-1522; b) P. V. Braun, P. Wiltzius, *Nature* **1999**, *402*, 603-604; c) C. I. Aguirre, E. Reguera, A. Stein, *Adv. Funct. Mater.* **2010**, *20*, 2565-2578.

[20] G. M. Miyake, R. A. Weitekamp, R. H. Grubbs, in *Handbook of Metathesis Vol. 3: Polymer Synthesis*, 2 ed. (Eds.: R. H. Grubbs, E. Knosravi), Wiley-VCH Verlag GmbH & Co, **2015**, pp. 93-113.

[21] M. B. Runge, C. E. Lipscomb, L. R. Ditzler, M. K. Mahanthappa, A. V. Tivanski, N. B. Bowden, *Macromolecules* **2008**, *41*, 7687-7694.

[22] Y. Fink, A. M. Urbas, M. G. Bawendi, J. D. Joannopoulos, E. L. Thomas, *J. Lightwave Tech.* **1999**, *17*, 1963-1969.

[23] F. S. Bates, G. H. Fredrickson, *Annu. Rev. Phys. Chem.* **1990**, *41*, 525-557.

[24] a) A. Walther, A. H. Müller, *Chem. Rev.* **2013**, *113*, 5194-5261; b) Y. Mai, A. Eisenberg, *Chem. Soc. Rev.* **2012**, *41*, 5969-5985.

[25] J. Rzayev, *Macromolecules* **2009**, *42*, 2135-2141.

[26] a) C. M. Bates, F. S. Bates, *Macromolecules* **2017**, *50*, 3–22; b) A. Noro, Y. Tomita, Y. Matsushita, E. L. Thomas, *Macromolecules* **2016**, *49*, 8971–8979.

[27] J. K. D. Mapas, T. Thomay, A. N. Cartwright, J. Ilavsky, J. Rzayev, *Macromolecules* **2016**, *49*, 3733-3738.

[28] S. W. Hong, W. Gu, J. Huh, B. R. Sveinbjörnsson, G. Jeong, R. H. Grubbs, T. P. Russel, *ACS Nano* **2013**, *7*, 9684-9692.

[29] A. M. Urbas, M. Maldovan, P. DeRege, E. L. Thomas, *Adv. Mater.* **2002**, *14*, 1850-1853.

[30] J. Rzayev, *ACS Macro Lett.* **2012**, *1*, 1146-1149.

[31] a) M. Zhang, A. H. E. Müller, *J. Polym. Sci., Part A: Polym. Chem.* **2005**, *43*, 3461-3481; b) S. S. Sheiko, M. Möller, *Chem. Rev.* **2001**, *101*, 4099-4123.

[32] a) M. Hu, Y. Xia, G. B. McKenna, J. A. Kornfield, R. H. Grubbs, *Macromolecules* **2011**, *44*, 6935-6943; b) B. M. Yavitt, Y. Gai, D.-P. Song, H. H. Winter, J. J. Watkins, *Macromolecules* **2016**; c) S. J. Dalsin, M. A. Hillmyer, F. S. Bates, *Macromolecules* **2015**, *48*, 4680-4691.

[33] W. Gu, J. Huh, S. W. Hong, B. R. Sveinbjörnsson, C. Park, R. H. Grubbs, T. P. Russell, *ACS Nano* **2013**, *7*, 2551-2558.

[34] S. J. Dalsin, T. G. Rions-Maehren, M. D. Beam, F. S. Bates, M. A. Hillmyer, M. W. Matsen, *ACS Nano* **2015**, *9*, 12233-12245.

[35] J. Bolton, T. S. Bailey, J. Rzayev, *Nano Lett.* **2011**, *11*, 998-1001.

[36] B. R. Sveinbjörnsson, *Ph.D. Dissertation*, California Institute of Technology (Pasadena, CA), April, **2014**.

[37] a) R. Verduzco, X. Li, S. L. Pesek, G. E. Stein, *Chem. Soc. Rev.* **2015**, *44*, 2405-2420; b) C. Feng, Y. Li, D. Yang, J. Hu, X. Zhang, X. Huang, *Chem. Soc. Rev.* **2001**, *40*, 1282-1295.

[38] S. S. Sheiko, B. S. Sumerlin, K. Matyjaszewski, *Prog. Polym. Sci.* **2008**, *33*, 759-785.

[39] a) H. Shinoda, K. Matyjaszewski, *Macromolecules* **2001**, *34*, 6243-6248; b) Y. Xia, B. D. Olsen, J. A. Kornfield, R. H. Grubbs, *J .Am. Chem. Soc.* **2009**, *131*, 18525-18532; c) Z. Li, K. Zhang, J. Ma, C. Cheng, K. L. Wooley, *J. Polym. Sci. A, Polym. Chem.* **2009**, *47*, 5557-5563.

[40] a) M. B. Runge, N. B. Bowden, *J. Am. Chem. Soc.* **2007**, *129*, 10551-10560; b) M. B. Runge, S. Dutta, N. B. Bowden, *Macromolecules* **2006**, *39*, 498-508.

[41] M. W. Matsen, F. S. Bates, *J. Polym. Sci., Part B: Polym. Phys.* **1997**, *35*, 945-952.

[42] a) Y. Xia, J. A. Kornfield, R. H. Grubbs, *Macromolecules* **2009**, *42*, 3761-3766; b) C. Cheng, E. Khoshdel, K. L. Wooley, *Macromolecules* **2005**, *38*, 9455-9465.

[43] M. Vayer, M. A. Hillmyer, M. Dirany, G. Thevenin, R. Erre, C. Sinturel, *Thin Solid Films* **2010**, *518*, 3710-3715.

[44] G. M. Miyake, R. A. Weitekamp, V. A. Piunova, R. H. Grubbs, *J. Am. Chem. Soc.* **2012**, *134*, 14249-14254.

[45] a) E. Yashima, K. Maeda, H. Iida, Y. Furusho, K. Nagai, *Chem. Rev.* **2009**, *109*, 6102-6211; b) S. Mayer, R. Zentel, *Prog. Polym. Sci.* **2001**, *26*, 1973-2013.

[46] J. T. Chen, E. L. Thomas, C. K. Ober, G.-p. Mao, *Science* **1996**, *273*, 343-336.

[47] M. Kikuchi, L. T. N. Lien, A. Narumi, Y. Jinbo, Y. Izumi, K. Nagai, S. Kawaguchi, *Macromolecules* **2008**, *41*, 6564-6572.

[48] a) N. A. Lynd, M. A. Hillmyer, *Macromolecules* **2005**, *38*, 8803-8810; b) N. A. Lynd, A. J. Meuler, M. A. Hillmyer, *Prog. Polym. Sci.* **2008**, *33*, 875-893; c) J. M. Widin, M. Kim, A. K. Schmitt, E. Han, P. Gopalan, M. K. Mahanthappa, *Macromolecules* **2013**, *46*, 4472-4480.

[49] V. A. Piunova, G. M. Miyake, C. S. Daeffler, R. A. Weitekamp, R. H. Grubbs, *J. Am. Chem. Soc.* **2013**, *135*, 15609-15616.

[50] a) K. Koo, H. Ahn, S.-W. Kim, D. Y. Ryu, T. P. Russell, *Soft Matter* **2013**, *9*, 9059; b) F. H. Schacher, P. A. Rupar, I. Manners, *Angew. Chem. Int. Ed.* **2012**, *51*, 7898-7921; c) J. Yoon, W. Lee, E. L. Thomas, *MRS Bulletin* **2011**, *30*, 721-726; d) A. C. Edrington, A. M. Urbas, P. DeRege, C. X. Chen, T. M. Swager, N. Hadjichristidis, M. Xenidou, L. J. Fetters, J. D. Joannopoulos, Y. Fink, E. L. Thomas, *Adv. Mater.* **2001**, *13*, 421-425.

[51] R. J. Macfarlane, B. Kim, B. Lee, R. A. Weitekamp, C. M. Bates, S. F. Lee, A. B. Chang, K. T. Delaney, G. H. Fredrickson, H. A. Atwater, R. H. Grubbs, *J. Am. Chem. Soc.* **2014**, *136*, 17374-17377.

[52] R. J. Spontak, N. P. Patel, in *Developments in Block Copolymer Science and Technology* (Ed.: I. W. Hamley), John Wiley & Sons, Ltd, Chichester, UK, **2004**.

[53] G. M. Miyake, V. A. Piunova, R. A. Weitekamp, R. H. Grubbs, *Angew. Chem. Int. Ed.* **2012**, *51*, 11246-11248.

[54] a) K. H. Ku, H. Yang, S. G. Jang, J. Bang, B. J. Kim, *J. Polym. Sci. Part A: Polym. Chem.* **2016**, *54*, 228-237; b) B. Sarkar, P. Alexandridis, *Prog. Polym. Sci.* **2015**, *40*, 33-62; c) I. W. Hamley, *Nanotech.* **2003**, *14*, R39-R54; d) M. R. Bockstaller, R. A. Mickiewicz, E. L. Thomas, *Adv. Mater.* **2005**, *17*, 1331-1349.

[55] a) D.-P. Song, S. Shahin, W. Xie, S. Mehravar, X. Liu, C. Li, R. A. Norwood, J.-H. Lee, J. J. Watkins, *Macromolecules* **2016**, *49*, 5068-5075; b) D. P. Song, C. Li, W. Li, J. J. Watkins, *ACS Nano* **2016**, *10*, 1216-1223; c) D. P. Song, C. Li, N. S. Colella, X. Lu, J. H. Lee, J. J. Watkins, *Adv. Optical Mater.* **2015**, *3*, 1169-1175; d) D. P. Song, Y. Lin, Y. Gai, N. S. Colella, C. Li, X. H. Liu, S. Gido, J. J. Watkins, *J. Am. Chem. Soc.* **2015**, *137*, 3771-3774.

[56] J. Polte, *CrystEngComm* **2015**, *17*, 6809-6830.

[57] D. P. Song, C. Li, N. S. Colella, W. Xie, S. Li, X. Lu, S. Gido, J. H. Lee, J. J. Watkins, *J Am Chem Soc* **2015**, *137*, 12510-12513.

[58] K. Kawamoto, M. Zhong, K. R. Gadelrab, L. C. Cheng, C. A. Ross, A. Alexander-Katz, J. A. Johnson, *J Am Chem Soc* **2016**, *138*, 11501-11504.

[59] a) D. R. Snoswell, A. Kontogeorgos, J. J. Baumberg, T. D. Lord, M. R. Mackley, P. Spahn, G. P. Hellmann, *Phys. Rev. E* **2010**, *81*, 020401; bA. J. Parnell, N. Tzokova, A. Pryke, J. R.

Howse, O. O. Mykhaylyk, A. J. Ryan, P. Panine, J. P. Fairclough, *Phys. Chem. Chem. Phys.* **2011**, *13*, 3179-3186.

[60] aY. Yue, J. P. Gong, *J. Photochem. and Photobio. C: Photochem. Rev.* **2015**, *23*, 45-67; b) J. E. Stumpel, D. J. Broer, A. P. Schenning, *Chem. Commun.* **2014**, *50*, 15839-15848; c) H. Wang, K. Q. Zhang, *Sensors* **2013**, *13*, 4192-4213.

[61] I. B. Burgess, M. Lončar, J. Aizenberg, *J. Mater. Chem. C* **2013**, *1*, 6075.

[62] C. Osuji, C.-Y. Chao, I. Bita, C. K. Ober, E. L. Thomas, *Adv. Funct. Mater.* **2002**, *12*, 753-758.

[63] a) H. Fudouzi, T. Sawada, *Langmuir* **2006**, *22*, 1365-1368; b) E. P. Chan, J. J. Walish, E. L. Thomas, C. M. Stafford, *Adv. Mater.* **2011**, *23*, 4702-4706; c) E. P. Chan, J. J. Walish, A. M. Urbas, E. L. Thomas, *Adv. Mater.* **2013**, *25*, 3934-3947.

[64] a) J. H. Holtz, S. A. Asher, *Nature* **1997**, *389*, 829-832; b) K. Lee, S. A. Asher, *J. Am. Chem. Soc.* **2000**, *122*, 9534-9537; c) Y.-J. Lee, P. V. Braun, *Adv. Mater.* **2003**, *15*, 563-566.

[65] a) X. Xu, G. Friedman, K. D. Humfeld, S. A. Majetich, S. A. Asher, *Chem. Mater.* **2002**, *14*, 1249-1256; b) K. Ueno, K. Matsubara, M. Wantanabe, Y. Takeoka, *Adv. Mater.* **2007**, *19*, 28087-22812.

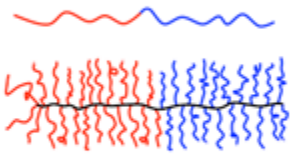

Figure 1. Comparison of linear (top) and bottlebrush (bottom) block copolymers.

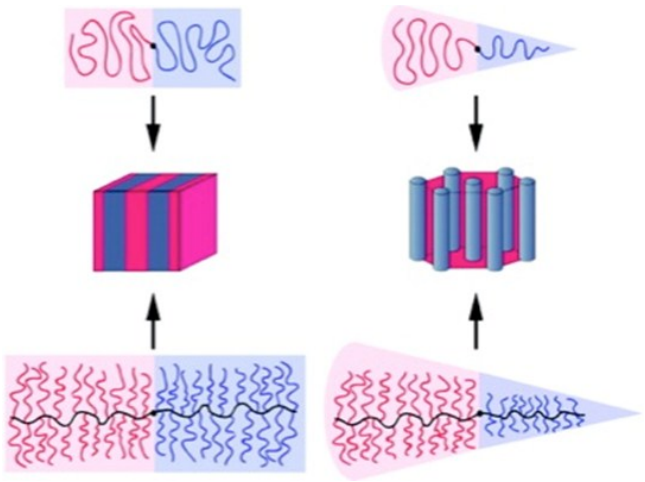

Figure 2. Comparison of ordered phases favored for linear (top) and bottlebrush (bottom) diblock copolymers. Cylindrical phases are favored by asymmetric block lengths for linear copolymers or brush lengths for bottlebrush copolymers. Reproduced with permission.[35] Copyright 2011, American Chemical Society.

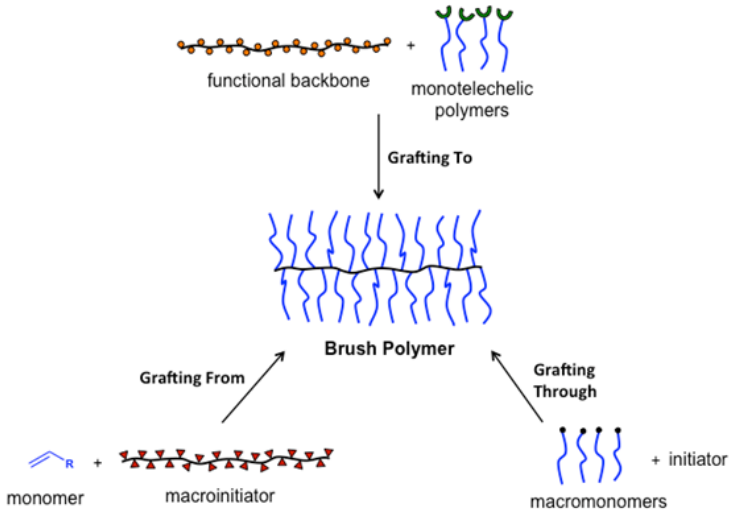

Figure 3. General synthetic methods to prepare brush polymers.

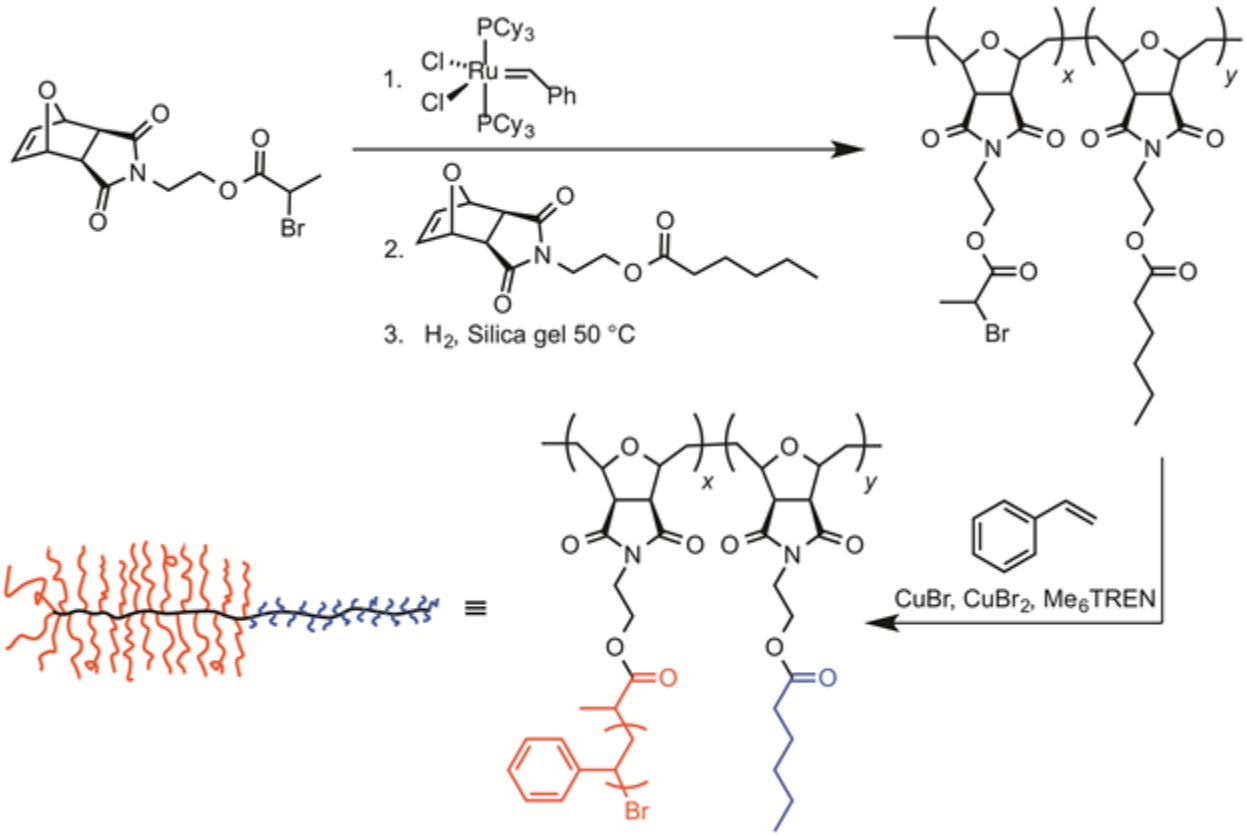

Figure 4. Synthesis of comb block copolymers with one PS-grafted block and one ungrafted block.

Table 1. Domain sizes and morphologies of polystyrene/hexanoate brush-coil copolymers.

Entry	*x*:*y*[a)]	Polystyrene (mol%)	Morphology[b)]	Domain size (nm)[b), c)]
1	100:2033	61	Lamellae	145 ± 26
2	250:2033	75	Cylinders	258 ± 27
3	150:1524	77	Cylinders	147 ± 18
4	450:2033	84	Spheres	226 ± 13
5	200:1016	89	Spheres	132 ± 7

[a]Ratio of the polystyrene-decorated backbone monomer, *x*, to the hexanoate-substituted monomer, *y*; [b] Determined by SEM; [c] The domain size is the repeat unit of the morphology; for cylinders and spheres, this is defined as the center-to-center spacing.

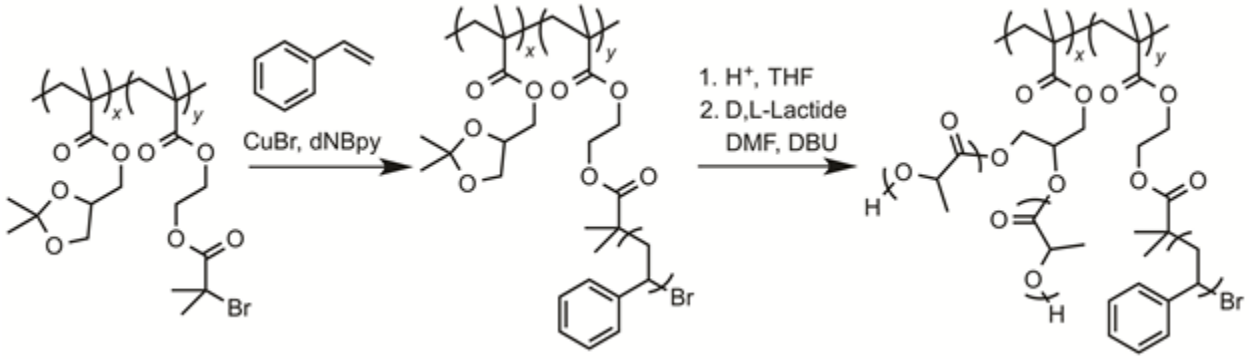

Figure 5. Grafting-from synthesis of polylactide/polystyrene brush block copolymers.

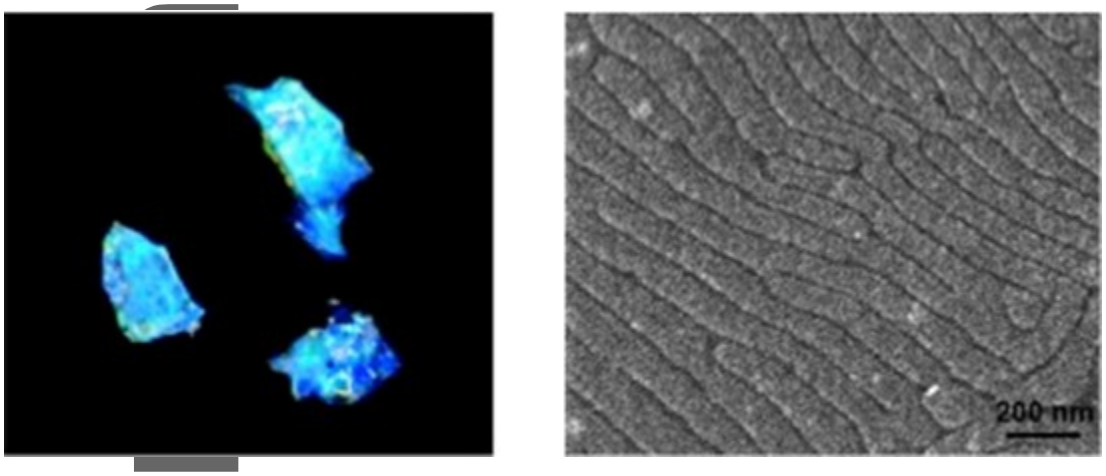

Figure 6. Reflection of blue light (left) and SEM image (right) of a polystyrene/polylactide bottlebrush block copolymer (M_n = 2400 kDa, f_{PLA} = 0.37). Reproduced with permission.[25] Copyright 2009, American Chemical Society.

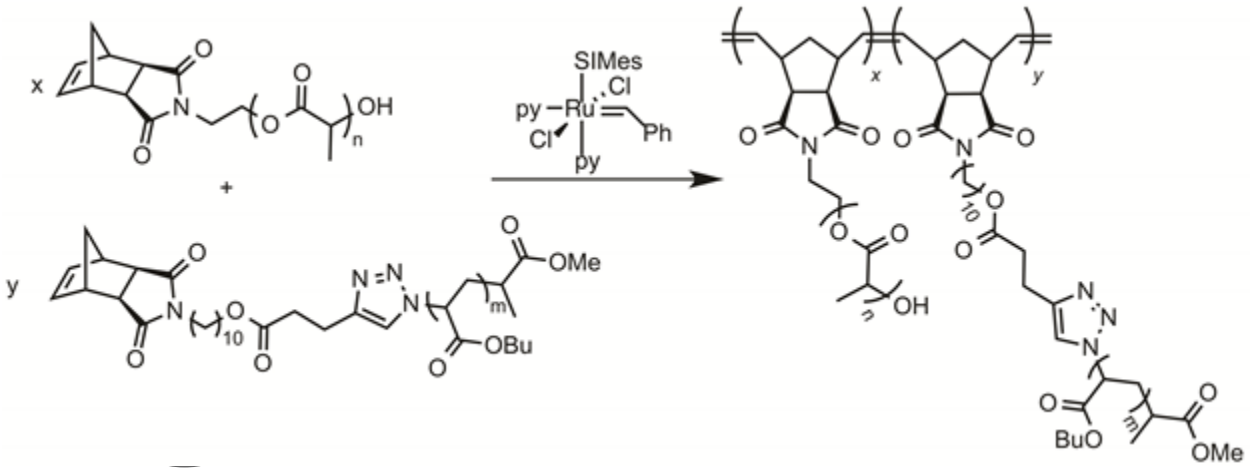

Figure 7. Synthesis of polylactide/poly(*n*-butylacrylate) bottlebrush copolymers by ROMP.

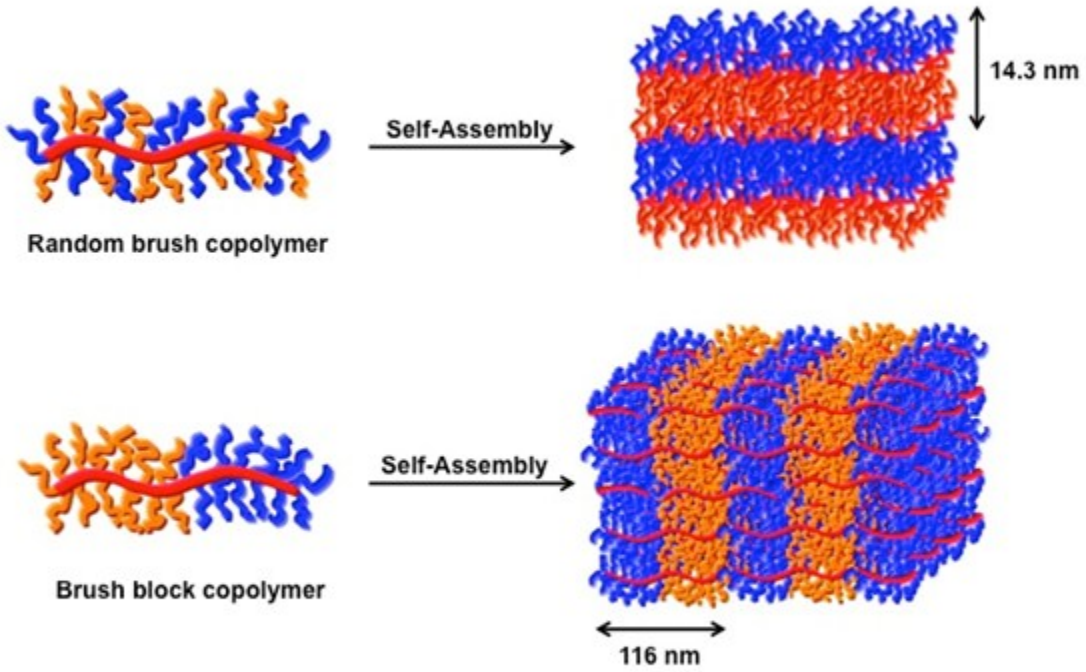

Figure 8. Assembly of symmetric brush random and block copolymers. Domain spacing is controlled by brush length for the random copolymers, while the brush copolymers assemble

with spacing dictated by the backbone length. Reproduced with permission.[39b] Copyright 2009, American Chemical Society.

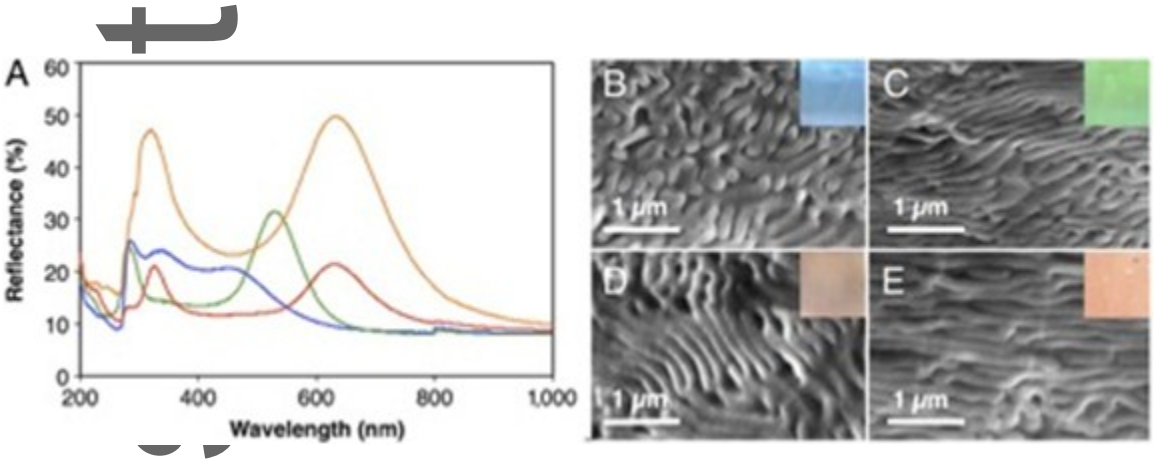

Figure 9. (A) Reflectance spectra for photonic crystal films (M_n = 2940 kDa) prepared by controlled evaporation from DCM (blue), THF (green), after thermal treatment (red), or by thermal annealing under compression (orange). SEM cross-sections of films prepared by (B) evaporation from DCM; (C, D) evaporation from THF before (C) and after (D) thermal annealing; and (E) direct thermal annealing under compression. The insets are photographs of the samples. Reproduced with permission.[7] Copyright 2012, National Academy of Sciences.

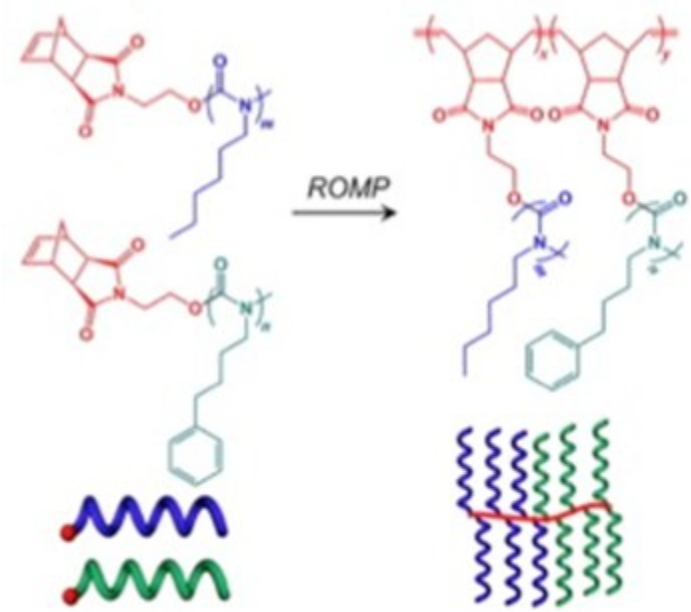

Figure 10. Synthesis of poly(isocyanate)-based brush block copolymers by ROMP. Depictions of rigid-rod helical poly(isocyanate) side chains are shown below the structures. Reproduced with permission.[44] Copyright 2012, American Chemical Society.

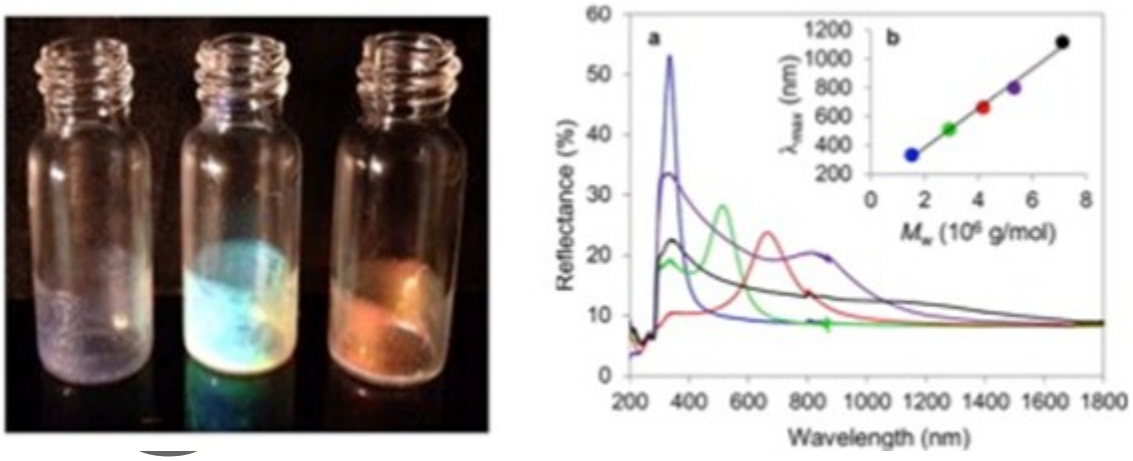

Figure 11. Left: Photograph of poly(isocyanate)-based photonic crystals prepared by controlled evaporation from DCM. Right: (a) Reflectance spectra for poly(isocyanate)-based BBCP thin films with M_w = 1512 (blue), 2918 (green), 4167 (red), 5319 (purple), and 7119 (black) kDa; (b) plot of λ_{max} as a function of M_w. Reproduced with permission.[44] Copyright 2012, American Chemical Society.

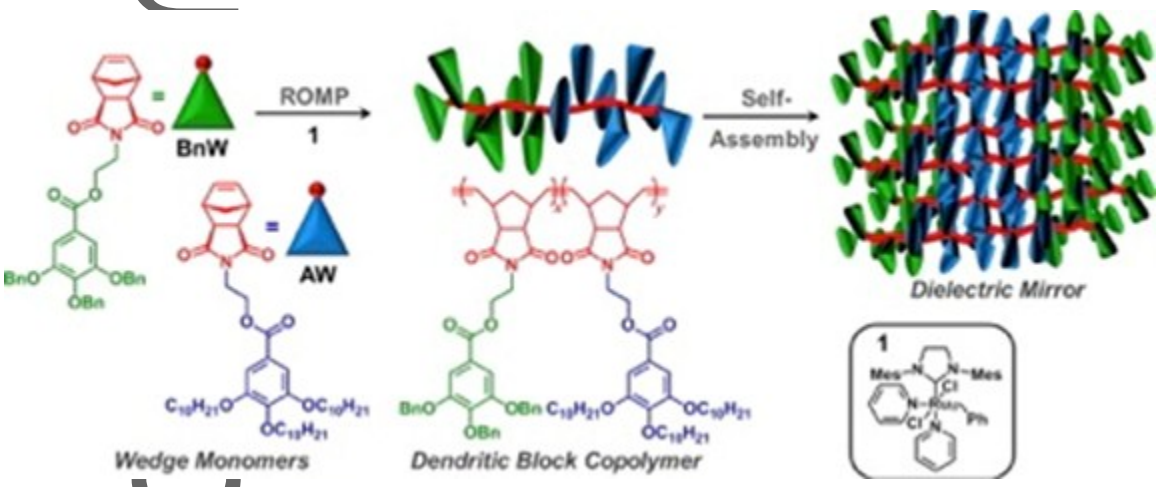

Figure 12. Synthesis of dendronized block copolymers by ROMP. Reproduced with permission.[49] Copyright 2013, American Chemical Society.

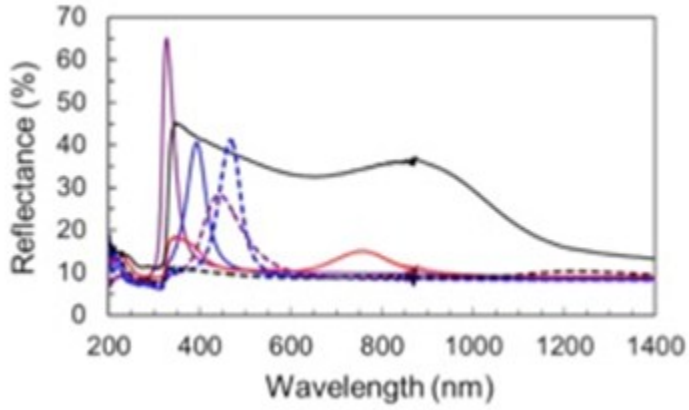

Figure 13. Plot of reflectance as a function of wavelength for dendronized block copolymer thin films with M_w = 480 kDa (purple), 570 kDa (blue), 1250 kDa (red), 1390 kDa (black). Samples were prepared by controlled evaporation (solid line) or thermal annealing (dashed line). Reproduced with permission.[49] Copyright 2013, American Chemical Society.

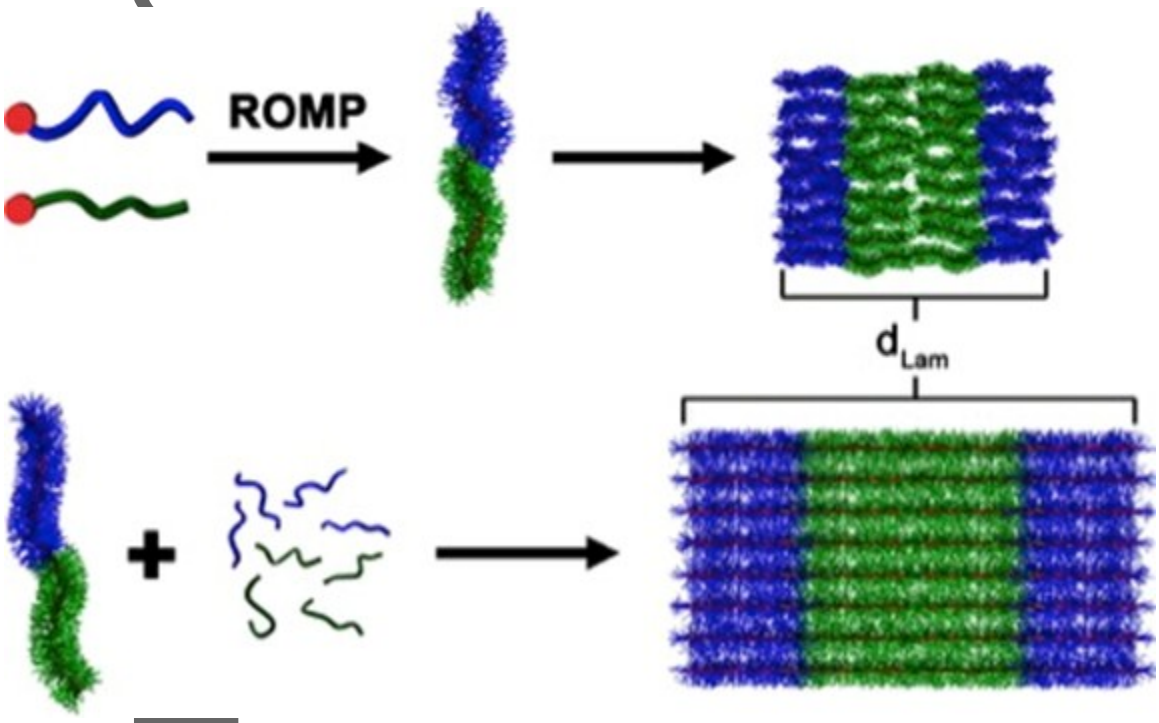

Figure 14. Synthesis and self-assembly of polystyrene/polylactide BBCPs to lamellar arrays. Addition of low molecular weight PS and PLA homopolymers swells these arrays and improves long range order. Reproduced with permission.[51] Copyright 2014, American Chemical Society.

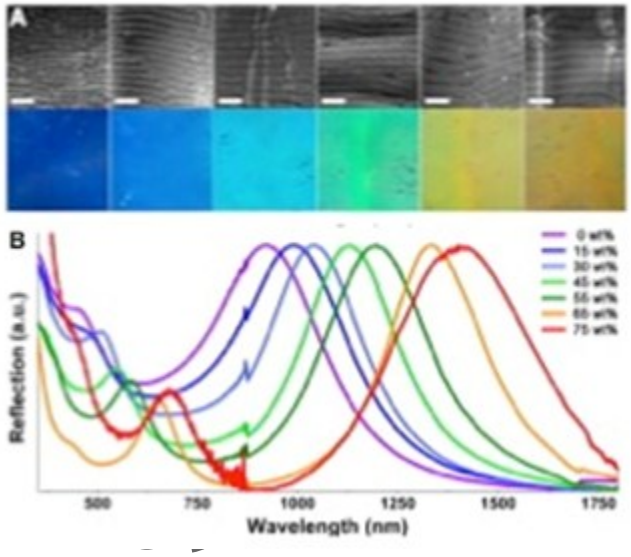

Figure 15. A) SEM images of PS-*b*-PLA BBCP film cross-sections with 0–67.5 wt% HP and corresponding photographs of colored films with increasing wavelengths of reflected light. Scale bars represent 550 nm. B) UV–Vis spectra of a BBCP blended with varying levels of HP showing improved ordering at low to moderate wt%. Reproduced with permission.[51] Copyright 2014, American Chemical Society.

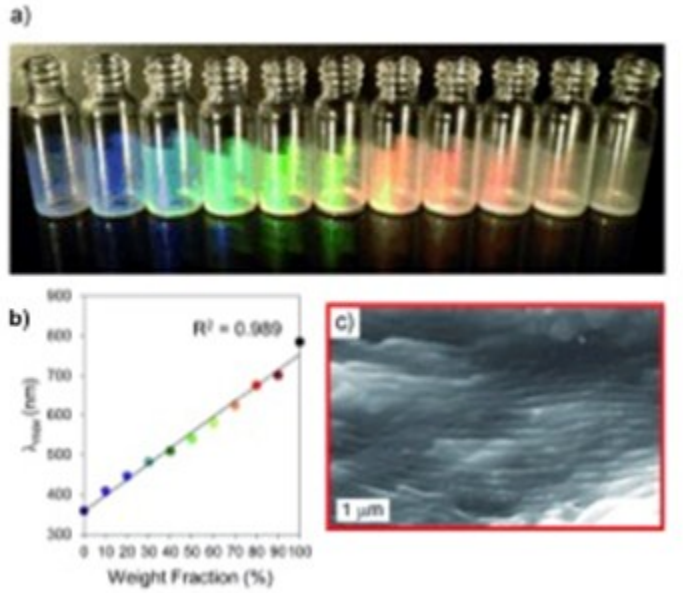

Figure 16. A) Photograph of films derived from blends of two BBCPs of different molecular weights at varying concentrations from 100% of one unblended polymer to 100% of the other. (B) Linear relationship suggesting the predictability of λ_{max} by manipulating blend ratio. (C) SEM image of a cross-section of an 80:20 blend of a low and high molecular weight BBCP. Reproduced with permission.[53] Copyright 2012, Wiley-VCH.

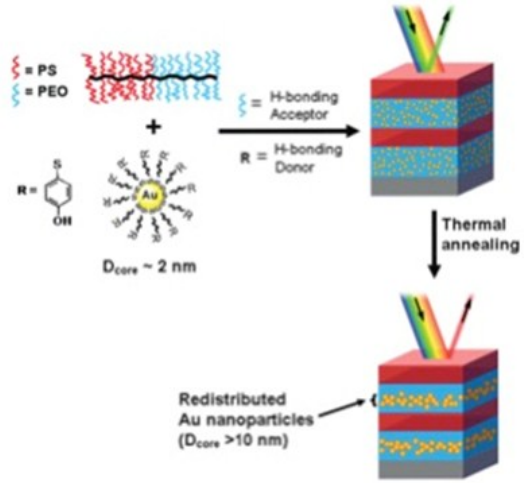

Figure 17. Selective incorporation of gold NPs into the PEO domains of a PS-*b*-PEO BBCP. Thermal annealing at 120 °C increases the size of the gold NPs and their distribution in the PEO layers, leading to a red shift in λ_{max}. Reproduced with permission.[55c] Copyright 2015, Wiley-VCH.

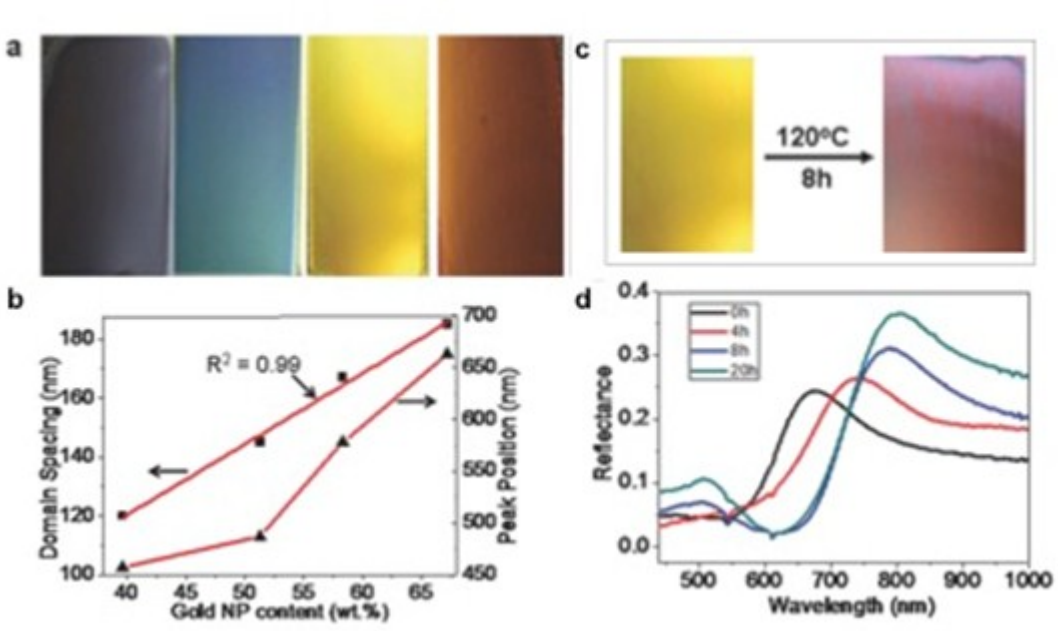

Figure 18. A) Images of nanocomposite films derived from the self-assembly of a BBCP with increasing gold NP loading concentrations. B) Changes in domain spacing and wavelength of reflection according to NP loading. C) Color change observed following thermal annealing and increased NP size. D) Kinetics of the effect of thermal annealing on wavelength of reflection. Reproduced with permission.[55c] Copyright 2015, Wiley-VCH.

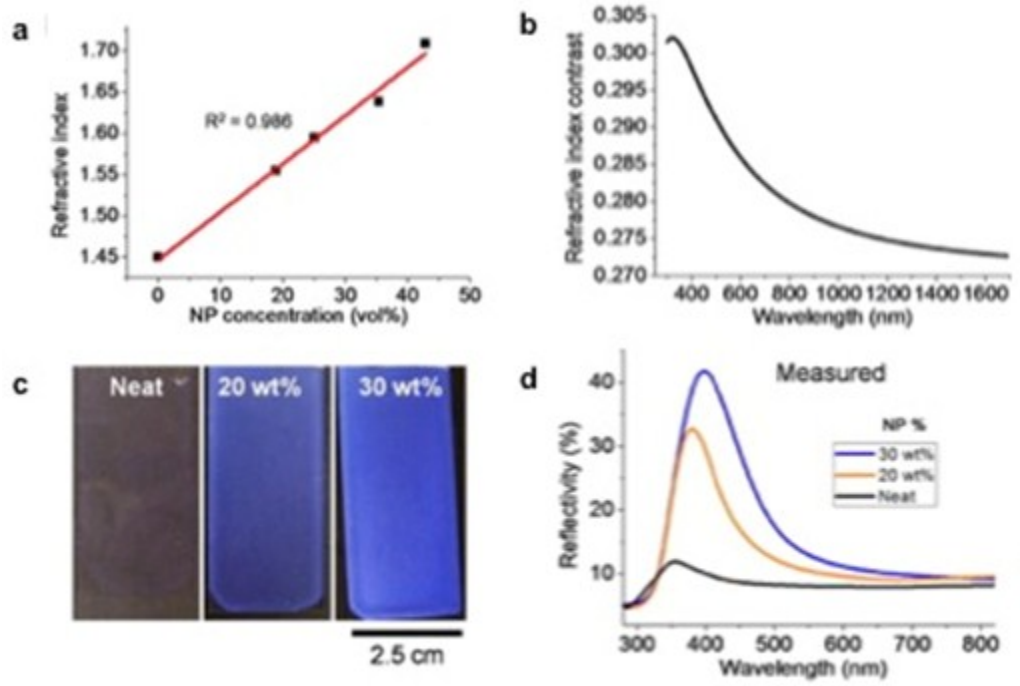

Figure 19. A) Increase in refractive index of the ZrO_2/PEO layer with increasing NP concentration. B) Refractive index contrast (Δn) between P*t*BA and NP/PEO at 70 wt% NP loading. C) Photographs of films derived from the self-assembly of a BBCP with increasing ZrO_2 NP loading, showing increased reflectivity (left to right). D) Enhanced reflectivity and longer peak wavelength of reflection with increasing wt% NP. Reproduced with permission.[55b] Copyright 2015, American Chemical Society.